

# First direct observation of coseismic slip and seafloor rupture along a submarine normal fault and implications for fault slip history

Javier Escartin, Frédérique E Leclerc, Jean-Arthur J Olive, Catherine Mevel, Mathilde Cannat, Sven E Petersen, Nico E Augustin, Nathalie Feuillet, Christine Deplus, Antoine Bézos, et al.

▶ **To cite this version:**

Javier Escartin, Frédérique E Leclerc, Jean-Arthur J Olive, Catherine Mevel, Mathilde Cannat, et al.. First direct observation of coseismic slip and seafloor rupture along a submarine normal fault and implications for fault slip history. Earth and Planetary Science Letters, 2016, 450, pp.96-107. 10.1016/j.epsl.2016.06.024 . insu-01557932

**HAL Id: insu-01557932**

**https://insu.hal.science/insu-01557932**

Submitted on 6 Jul 2017

**HAL** is a multi-disciplinary open access archive for the deposit and dissemination of scientific research documents, whether they are published or not. The documents may come from teaching and research institutions in France or abroad, or from public or private research centers.

L'archive ouverte pluridisciplinaire **HAL**, est destinée au dépôt et à la diffusion de documents scientifiques de niveau recherche, publiés ou non, émanant des établissements d'enseignement et de recherche français ou étrangers, des laboratoires publics ou privés.

Earth and Planetary Science Letters 450 (2016) 96–107

Contents lists available at ScienceDirect

Earth and Planetary Science Letters

www.elsevier.com/locate/epsl

# First direct observation of coseismic slip and seafloor rupture along a submarine normal fault and implications for fault slip history

Javier Escartín [a,*], Frédérique Leclerc [b], Jean-Arthur Olive [c], Catherine Mevel [a], Mathilde Cannat [a], Sven Petersen [d], Nico Augustin [d], Nathalie Feuillet [a], Christine Deplus [a], Antoine Bezos [e], Diane Bonnemains [a], Valérie Chavagnac [f], Yujin Choi [a], Marguerite Godard [g], Kristian A. Haaga [h], Cédric Hamelin [h], Benoit Ildefonse [g], John W. Jamieson [d], Barbara E. John [i], Thomas Leleu [f], Christopher J. MacLeod [j], Miquel Massot-Campos [k], Paraskevi Nomikou [l], Marine Paquet [a], Céline Rommevaux-Jestin [a], Marcel Rothenbeck [d], Anja Steinführer [d], Masako Tominaga [m], Lars Triebe [b], Ricard Campos [n], Nuno Gracias [n], Rafael Garcia [n], Muriel Andreani [o], Géraud Vilaseca [a]

[a] Institut de Physique du Globe de Paris (CNRS UMR7154), Paris, France
[b] Earth Observatory of Singapore, Singapore
[c] Lamont-Doherty Earth Observatory, Palisades, NY, United States
[d] GEOMAR Helmholtz Centre for Ocean Research, Kiel, Germany
[e] University of Nantes, Nantes, France
[f] Géosciences Environnement Toulouse (CNRS UMR5563), Toulouse, France
[g] Géosciences Montpellier, University of Montpellier, France
[h] University of Bergen, Bergen, Norway
[i] University of Wyoming, Laramie, WY, United States
[j] Cardiff University, Cardiff, Wales, United Kingdom
[k] University of the Balearic Islands, Palma de Majorca, Spain
[l] University of Athens, Athens, Greece
[m] Texas A&M University, College Station, TX, United States
[n] University of Girona, Girona, Spain
[o] University of Lyon, Lyon, France

ARTICLE INFO

*Article history:*
Received 2 January 2016
Received in revised form 3 May 2016
Accepted 16 June 2016
Available online 30 June 2016
Editor: A. Yin

*Keywords:*
submarine fault
surface rupture
earthquake
fault slip
neotectonics
microbathymetry

ABSTRACT

Properly assessing the extent and magnitude of fault ruptures associated with large earthquakes is critical for understanding fault behavior and associated hazard. Submarine faults can trigger tsunamis, whose characteristics are defined by the geometry of seafloor displacement, studied primarily through indirect observations (e.g., seismic event parameters, seismic profiles, shipboard bathymetry, coring) rather than direct ones. Using deep-sea vehicles, we identify for the first time a marker of coseismic slip on a submarine fault plane along the Roseau Fault (Lesser Antilles), and measure its vertical displacement of ~0.9 m in situ. We also map recent fissuring and faulting of sediments on the hangingwall, along ~3 km of rupture in close proximity to the fault's base, and document the reactivation of erosion and sedimentation within and downslope of the scarp. These deformation structures were caused by the 2004 $M_w$ 6.3 Les Saintes earthquake, which triggered a subsequent tsunami. Their characterization informs estimates of earthquake recurrence on this fault and provides new constraints on the geometry of fault rupture, which is both shorter and displays locally larger coseismic displacements than available model predictions that lack field constraints. This methodology of detailed field observations coupled with near-bottom geophysical surveying can be readily applied to numerous submarine fault systems, and should prove useful in evaluating seismic and tsunamigenic hazard in all geodynamic contexts.

© 2016 The Authors. Published by Elsevier B.V. This is an open access article under the CC BY license (http://creativecommons.org/licenses/by/4.0/).

* Corresponding author.
*E-mail address:* escartin.javier@gmail.com (J. Escartín).

http://dx.doi.org/10.1016/j.epsl.2016.06.024
0012-821X/© 2016 The Authors. Published by Elsevier B.V. This is an open access article under the CC BY license (http://creativecommons.org/licenses/by/4.0/).

## 1. Introduction

Seismically active faults routinely experience ruptures that propagate all the way to the Earth's surface. The earthquake surface rupture is characterized by its extent, nature and displacement pattern. It results from a complex combination of parameters, including fault geometry and segmentation, surface geology, fault slip history, or the dynamics and geometry of the seismic rupture at depth. Past and modern coseismic fault ruptures can be readily observed in subaerial environments through field observations, high-resolution microtopography, aerial photography, and satellite imagery, among other methods (e.g., Avouac et al., 2014; DePolo et al., 1991; Klinger, 2005). These detailed studies help constrain the seismogenic history of these faults, and document the accommodation and release of stress and strain (Bhat et al., 2007; King, 2005; Rockwell and Klinger, 2013).

Surface fault rupture studies have been critical to establish scaling laws between earthquake magnitude and observables such as maximum or average faults, displacement and rupture length (e.g., Papazachos et al., 2004; Wesnousky, 2006, 2008). These complement similar scaling laws based solely on subsurface ruptures (Scholz et al., 1986; Wells and Coppersmith, 1994). These seismic scaling laws primarily rely on strike-slip earthquakes, yet may depend strongly on fault type (Stock and Smith, 2000). In this context, normal fault ruptures appear largely under-represented. Owing to the complexity of fault rupture propagation and subsurface geological controls, the surface rupture is typically shorter than the subsurface one, and the data used to constrain these scaling laws suffer from significant scatter (e.g., Wells and Coppersmith, 1994). Predictions of earthquake properties can thus vary by an order of magnitude or more, depending on the fault rupture parameter considered.

While ∼70% of the Earth's seismicity occurs offshore, detailed fault surface rupture observations and associated studies to date are exclusively subaerial. Submarine ruptures can also be associated with tsunami hazard, a threat that has proven to be much more damaging for coastal areas than the earthquakes themselves (Marano et al., 2010). Seafloor observations of coseismic fault ruptures are thus needed to determine whether subaerial observations and associated scaling laws can be extrapolated to the marine environment. Seafloor rupture observations are effectively lacking owing to limitations imposed by the environment, the technological requirements to conduct detailed fieldwork, and the lack of observations prior to seismic events to identify and characterize subsequent coseismic ruptures.

Submarine earthquake geology and history is typically reconstructed from sedimentary records containing turbidities cored offshore and primarily along active margins (e.g., Beck et al., 2012; Goldfinger, 2011, and references therein). High-resolution seismic imaging of co-seismically deposited units can provide information on earthquake activity at greater depths (and therefore on longer timescales) than those probed by coring. However, these techniques do not characterize the rupture induced by individual earthquakes. So far, shipboard geophysical methods (bathymetry, side-scan sonar images) have been used to map recently reactivated faults (Armijo et al., 2005; Cattaneo et al., 2012; Elias et al., 2007), and to evaluate seafloor vertical displacement in the case of extremely large events such as the Tohoku-Oki earthquake (Fujiwara et al., 2011; Kodaira et al., 2012). Seafloor observations have also identified possible submarine coseismic scarps (Armijo et al., 2005; Matsumoto et al., 2009; Tsuji et al., 2012), but extensive seafloor characterizations of fault rupture extent and slip distribution are still lacking.

This study presents high-resolution geophysical data acquired in December 2013 along the Roseau fault, an active normal fault that produced a $M_w$ 6.3 earthquake in 2004 in the Guadeloupe archipelago (French West Indies, Fig. 1). Our data analysis demonstrates an unequivocal link between observed deformation structures and this seismic event allowing us to characterize the distribution and nature of the coseismic fault rupture at the seafloor, and to identify possible links between coseismic fault reactivation and erosional or depositional processes along the submarine fault scarp. We also measure the magnitude of coseismic displacement at a specific outcrop along the fault. Our results validate model predictions of fault rupture and tsunami generation in the area, and are compared with subaerial observations of normal fault rupture and associated scaling laws. We also demonstrate the feasibility of high-resolution seafloor mapping, and its importance for expanding our understanding of fault rupture and dynamics to the marine environment.

## 2. Intra-arc active faulting and seismicity: Les Saintes Graben (French Antilles)

The Les Saintes graben extends between Guadeloupe and Dominica Islands (Fig. 1) accommodating internal deformation of the Lesser Antilles arc due to oblique plate convergence (Feuillet et al., 2002, 2011a). This graben shows a long history of interacting volcanic emplacement and faulting, and is bound to the southwest by the ∼40 km long, NE dipping Roseau Fault (RF), which is segmented into several ∼5–15-km long portions (Fig. 1B). In its northern part, these are arranged as right-stepping echelons, trending N140°E, and crosscutting the seafloor in the vicinity of the Les Saintes archipelago, which is highly populated and a major tourist destination. The southern Roseau Fault section instead shows left-stepping echelons, with an overall trend of N120°E (Leclerc et al., in press).

The cumulative fault scarp height varies along the Roseau Fault trace and peaks at >150 m at its center, coinciding with the most prominent echelon, hereafter termed the Roseau echelon. The cumulative scarp dissects the flank of the volcanic arc, which slopes towards the southwest, and captures sediments from the Les Saintes Islands and adjacent reef platform, which are then channeled along the base of the Roseau scarp. These sediments, together with debris from the fault scarp, make up a >300-m thick layer within the hangingwall basin (Leclerc et al., in press).

On November 21st, 2004, the $M_w$ 6.3 Les Saintes earthquake struck the Guadeloupe archipelago, one of the strongest earthquakes to have occurred on French territory in the last decades. Ground shaking up to intensity-VIII was felt on Terre-de-Bas (Cara et al., 2005), triggering landslides and ground fissuring that seriously damaged ∼50% of the buildings (Feuillet et al., 2011a). The ∼10 km deep epicenter was located offshore, ∼15 km SE of the Les Saintes plateau (Fig. 1B). Relocation of the aftershock sequence indicates that this mainly extensional $M_w$ 6.3 earthquake ruptured the Roseau fault, which dips at ∼55° to the NE at depth (Bazin et al., 2010; Feuillet et al., 2011a). This triggered a tsunami with a maximum run-up of 3.5 m on the nearby coasts of Les Saintes archipelago (Le Friant et al., 2008). Lacking direct observations, ad-hoc models of fault slip and tsunami sources were used to estimate a seafloor rupture with an along-strike extent ranging between <10 km and ∼15 km, and normal displacements of up to 1 m, with an average of 0.3–0.6 m (Feuillet et al., 2011a; Le Friant et al., 2008). The focal mechanisms of both the main shock and the largest aftershocks indicate extension in the NE quadrant. The modeled rupture rake shows that the main event also accommodated a minor left-lateral slip component (Feuillet et al., 2011a). Aftershocks occurred mainly north of the original hypocenter, beneath Les Saintes plateau and along the northern echelons of the Roseau fault, in response to a static stress increase at the tip of the rupture (Feuillet et al., 2011a). In particular, the strongest aftershocks, 8–12 km deep and reaching $M_w$ up to 5.8, did not trigger

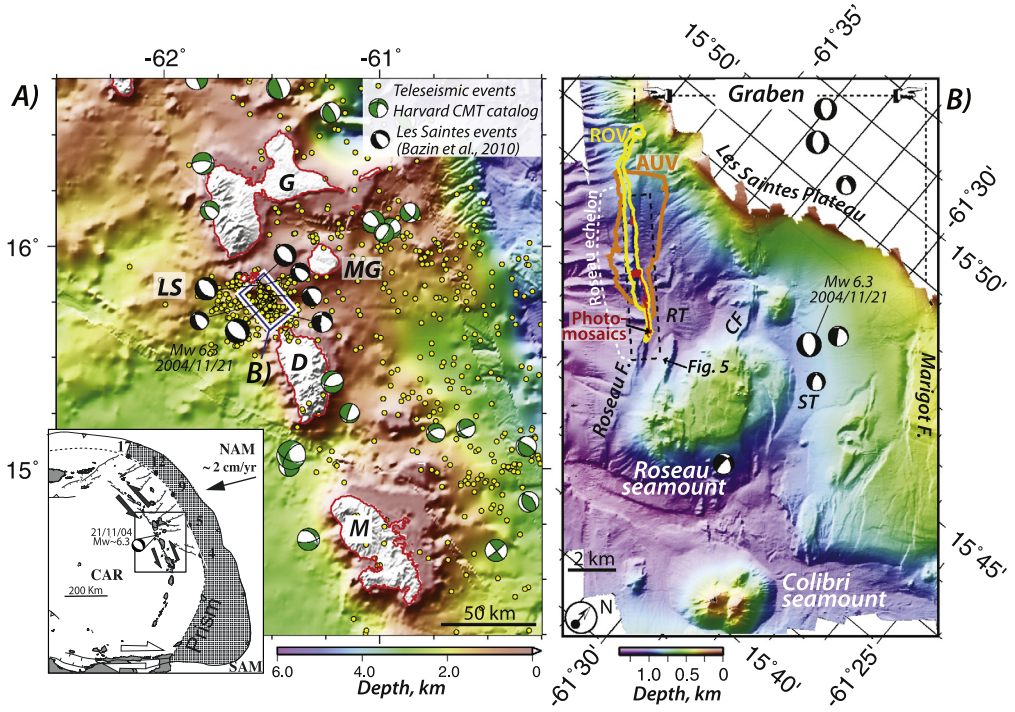



**Fig. 1.** A) Shipboard and satellite-derived bathymetry of the Antilles arc, showing the intra-arc seismicity (epicenters <50 km depth, thus excluding the subduction zone), and focal mechanisms (in green from the Harvard CMT catalog, in black from Bazin et al., 2010) showing intraplate normal fault mechanisms. The box corresponds to B). G: Guadeloupe I.; LS: Les Saintes I.; MG: Marie Galante Island; D: Dominica; M: Martinique. The inset shows the geodynamic context, with the trench parallel component of shear increases from 4 to 17 mm/yr between Martinique and Saba owing to convergence between the North and South American plates (NAM-SAM) and the Caribbean one (CAR); see details in Feuillet et al. (2010). B) Shipboard bathymetry of the graben system from cruise BathySaintes between Les Saintes Islands and Dominica, bound to the southwest by the Roseau Fault. The outline of the AUV and ROV microbathymetric surveys (orange and yellow outlines, respectively), seafloor photomosaics (red) along the Roseau fault, and location of Fig. 5 (dashed black box) are shown. The seismicity of the area and the focal mechanisms including the 21/11/2004 Les Saintes earthquake, that ruptured the Roseau Fault triggering a local tsunami (Feuillet et al., 2011a; Le Friant et al., 2008; Leclerc et al., in press), are also shown. RT: Roseau Trough; CF: Coche Fault; ST: Savane Trough. (For interpretation of the references to color in this figure legend, the reader is referred to the web version of this article.)

tsunamis, suggesting no surface break. In the main shock epicentral area, two aftershocks of $M_w$ 5 and 5.3 occurred within the first two weeks, and occurred at depths of 10 and 10.6 km. Once again, no tsunamis were triggered by these events, suggesting that the rupture did not reach the seafloor.

The 2004 earthquake is the first important seismic event to have occurred during the instrumental period along the Les Saintes fault system. Historical reports spanning the last 200 years do not mention other seismic events of similar size or larger in this archipelago (see Feuillet et al., 2011b, for a review of historical seismicity in the Lesser Antilles arc). Investigations of the fault trace are thus necessary to better apprehend the seismic behavior of this fault, and evaluate the associated hazards. Furthermore, extension in intra-arc domains is common, with numerous earthquakes showing normal focal mechanisms (e.g., Fabbri and Fournier, 1999; Galgana et al., 2007). Studies of submarine faults accommodating this intra-arc deformation can contribute to the understanding of their deformation history and to improving risk assessment for nearby coastal areas.

## 3. Data collection and analysis

To study and document the morphology, evolution, and deformation structures associated with a submarine intra-arc normal fault, including recent (coseismic) deformation, we conducted near-bottom, high resolution geophysical surveys along the trace of the Roseau Fault, which bounds to the southwest the graben linking Les Saintes and Dominica, and is sub-parallel to the subduction front (Fig. 1). We deployed both the autonomous underwater vehicle (AUV) Abyss (Geomar, Germany) and the remotely-operated vehicle (ROV) Victor6000 (Ifremer, France) during the 2013 ODEMAR cruise onboard Research Vessel Pourquoi pas? (French Oceanographic Cruises, http://dx.doi.org/10.17600/13030070). AUV and ROV vehicles collected near-bottom high resolution microbathymetry data (Fig. 1B), and dives were planned using previous shipboard multibeam bathymetry data acquired during the 2010 BATHYSAINTES cruise (French Oceanographic Cruises, http://dx.doi.org/10.17600/13030020). ROV surveys also acquired still electronic images to generate seafloor photomosaics (Prados et al., 2012) over >180,000 $m^2$ of seafloor (Fig. 1B), as well as high-resolution video imagery from a fault surface outcrop to generate high-resolution terrain models with texture-mapped imagery (Nicosevici and Garcia, 2013) (Figs. 2B and 3).

### 3.1. Bathymetry

Shipboard bathymetry around Les Saintes islands (Fig. 1B) was processed and gridded at 10 m/pixel; cruise and data details are provided elsewhere (Leclerc, 2014; Leclerc et al., 2014, in press). High-resolution, near-bottom bathymetry data were acquired using 200 kHz Reson Seabat 7125 multibeam systems installed on both underwater vehicles. The AUV survey, conducted at ~70 m above seafloor, covered an area of 9.6 $km^2$, providing detailed mapping of both the Roseau fault scarp and the adjacent hangingwall and footwall (Fig. 1B). ROV microbathymetric surveys were conducted during two dives flown at ~50 and ~10 m above seafloor, covering 3.1 $km^2$ of seafloor (Fig. 1B). Data were pre-processed with a vehicle re-navigation using MBSYSTEM, and manually cleaned and adjusted using both MBSYSTEM and Fledermaus Pro. AUV data were gridded at 2 m/pixel. ROV data were gridded at different resolutions depending on survey altitude, from ~25 cm/pixel for surveys at ~50 m above the seafloor, to ~10 cm/pixel for surveys

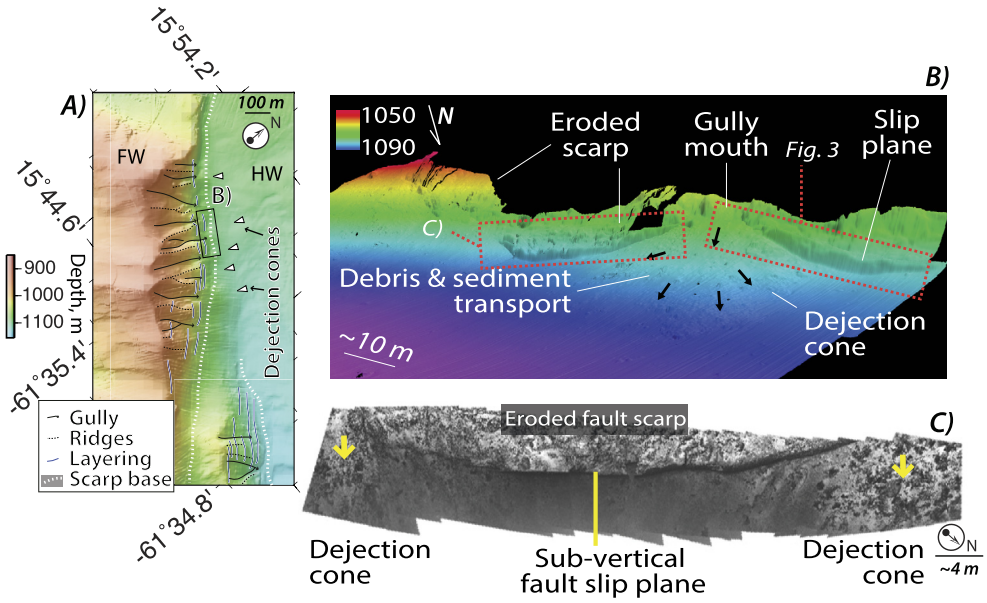



**Fig. 2.** A) Detail of the Roseau Fault scarp (AUV bathymetry) showing the gullies running perpendicular to the fault scarp, with the associated dejection cones at its base and depositing at the hangingwall. The fault scarp shows steps due to differential erosion of internal layering of footwall rocks (layered volcanic deposits, blue thin lines). FW: Footwall; HW: Hangingwall. B) Detail perspective view from ROV bathymetry of two sub-vertical fault slip planes at the base of the eroded Roseau scarp, laterally bound by gullies and the associated dejection cones. The position of the photomosaic in C) and the imaged fault slip plane in Fig. 3 are indicated (red dashed boxes). Scale bar is approximate owing to perspective. C) Photomosaic showing a vertical view of a sub-vertical fault slip plane, with debris and rock blocs at the mouth of gullies at each side of the fault slip plane. The mosaic also shows the degraded fault scarp above the fault slip plane (see also B). (For interpretation of the references to color in this figure legend, the reader is referred to the web version of this article.)

at ~10 m above seafloor, corresponding to photomosaic surveys (see below).

### 3.2. Seafloor mosaics

During surveys conducted by the ROV at 10 m above seafloor we used a vertically-mounted, low-light black-and-white camera to systematically acquire electronic still images of the seafloor. Individual images were first corrected for illumination and geometric distortion. Feature-matching between images was used to calculate camera motion and renavigate the ROV vehicle. Images were then projected and blended (Prados et al., 2012) to construct a geographically registered photomosaic with a pixel resolution of ~10 mm or better (Figs. 1B, 2C, and 4).

Mosaics were interpreted using both the available oblique video imagery from the ROV and the onboard scientific observations and descriptions, with methods developed in prior studies using similar datasets (Barreyre et al., 2012). Features of interest, primarily cracks in the sedimented footwall and at the base and summit of the fault scarp were manually digitized from the georeferenced photomosaics.

### 3.3. Videomosaics and three-dimensional terrain models from video imagery

Using the high-definition video camera system of ROV VICTOR, we conducted a systematic survey of a sub-vertical fault outcrop ~20 m wide and ~5 m high (Figs. 2B and 3). Video imagery was acquired sub-perpendicular to the fault plane, along horizontal and vertical overlapping video transects. Video imagery was first corrected to improve image quality (illumination, equalization, color shift), and processed to create a three-dimensional terrain model of the outcrop using structure from motion techniques (Campos et al., 2015). The video imagery is texture-mapped to the resulting three-dimensional terrain model, allowing us to directly digitize and measure features and structures visible in the imagery (Fig. 3). The resulting video-derived terrain model has a resolution that is better than that of models derived from acoustic multibeam data (<10 cm instead of 2 m to a minimum of 10 cm), and allows the mapping of sub-vertical and complex structures that cannot be properly imaged by conventional acoustic methods.

## 4. Results and interpretation

### 4.1. Morphology of the Roseau fault scarp

The microbathymetry and seafloor imagery highlight significant erosion and mass wasting along the cumulative scarp of the Roseau fault, with development of channels and deposition of material at the base of the scarp, generally in the form of dejection cones. Intense footwall incision is best developed where the scarp is highest, and where its slope averages 30–45° (Fig. 2A). Sections of the fault with less erosion, where the scarp is lower, show slopes approaching 70°. Gullies in this area shown in Fig. 2A are 10–20 m deep and spaced ~50–100 m apart, with some of the channels coalescing. The debris shed along the scarp is emplaced at the mouth of these gullies forming dejection cones on the hangingwall along the scarp base (Figs. 2A, B). These structures have a relief of up to 10–20 m, and are not visible in the shipboard bathymetry (Fig. 1B). Microbathymetry also reveals a stair-case scarp morphology, with laterally continuous steps decimeters to meters high (blue lines in Fig. 2A), which correspond to layered volcanic deposits within the footwall that have been uplifted by the Roseau Fault (Leclerc et al., in press), and enhanced by scarp erosion. The volcanic nature of this layering is also confirmed by a single vesicular lava sample showing fresh plagioclase phenocrysts, recovered during an ROV dive, and by geological observations at this sampling location and elsewhere along the scarp.

### 4.2. Vertical fault slip planes

Despite pervasive scarp degradation, the ROV microbathymetry and photomosaics reveal several sub-vertical scarps along the

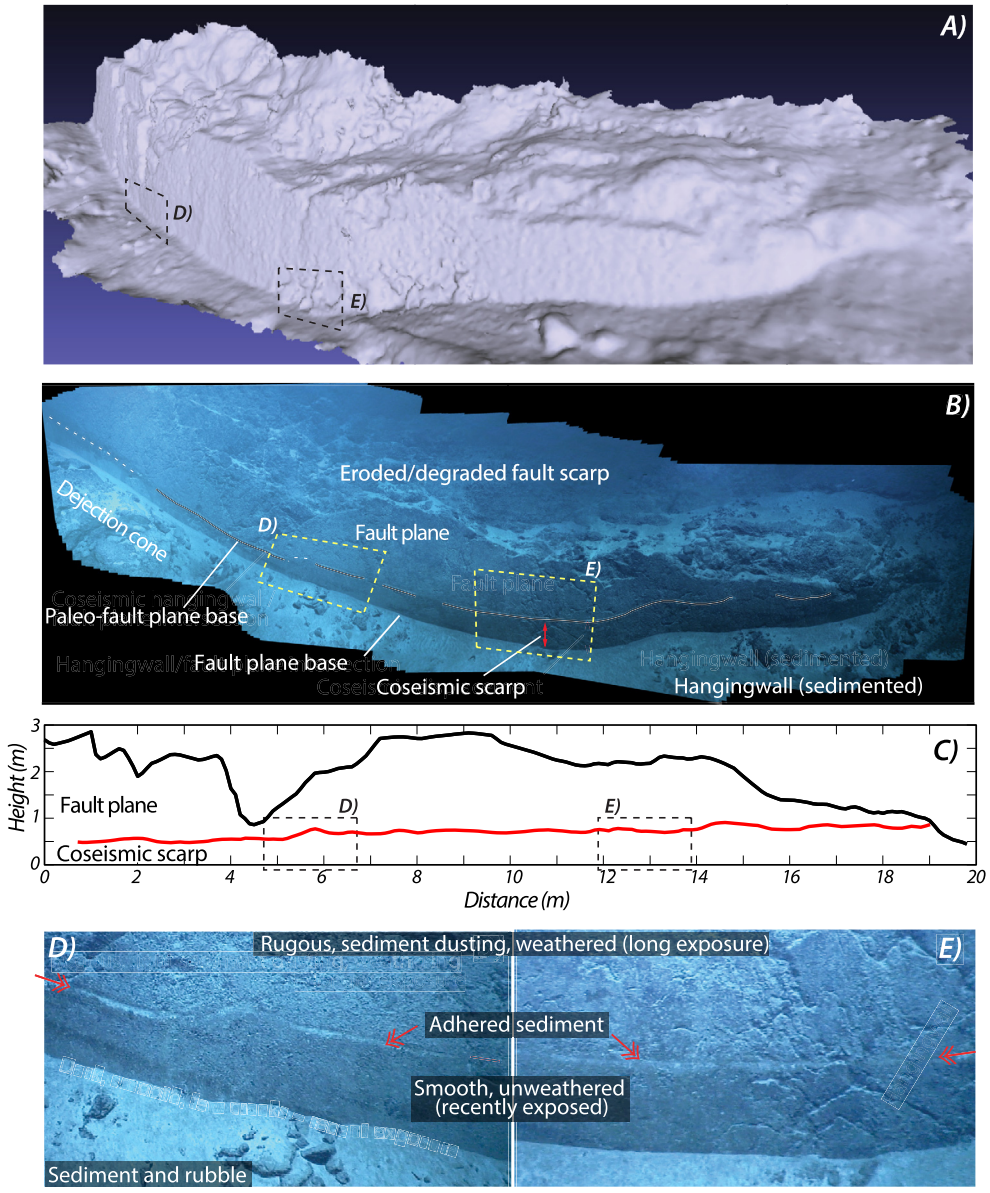



**Fig. 3.** (A) Video-derived three-dimensional terrain reconstruction of an exposed, subvertical fault slip plane (right slip plane in Fig. 2B), and (B) videomosaic of the same outcrop with interpretation of features overlain. The reconstruction is ~20 m long, with actual vertical scaling shown in C. C) Coseismic displacement, measured from the height of the coseismic slip (red line), shows a maximum of ~0.9 m along the preserved fault slip surface, that has a maximum height of ~3 m (black line). (D) and (E) show close-ups of the base of the fault free-plane (location shown in A, B, and C), showing a ribbon of slip surface exposed during the 2004 seismic event (coseismic scarp) bound by a line of sediment adhered to the slip plane. (For interpretation of the references to color in this figure legend, the reader is referred to the web version of this article.)

~3 km of surveyed fault strike (Figs. 2B, C). Each of these scarps can reach heights of up to 10 m, and extend between ~20 m and up to ~50 m laterally, often lying between the mouths of gullies, and in some cases show a mild curvature that in plane-view can have an across-fault amplitude of a few meters (Figs. 2B, C). The visual observations from ROV imagery of these sub-vertical planes reveal a smooth, polished surface (Figs. 2C and 3). We interpret these surfaces as exposed and preserved fault slip planes that have not yet been degraded by erosion. This interpretation is based on (1) the position of these slip planes at the base of the main cumulative Roseau Fault scarp, (2) their preferential preservation between the mouths of gullies, and hence away from areas displaying the most intense erosion, and (3) their overall geometry, with a smooth, high angle surface consistent with a fault plane that is breaching the surface at a steep dip (~70–80°).

### 4.3. Fault slip plane texture and earthquake-related vertical displacement

The systematic ROV video survey of one of the preserved fault planes (Fig. 3) allows us to characterize its morphology and texture in detail, so as to investigate its nature and, for the first time in a submarine fault slip plane, its seismic history. Figs. 3A and B show the video-derived terrain model and the videomosaic of a ~20 m long section of one of these fault slip planes, which shows a ~3 m high, subvertical fault surface. As in the case of the adjacent fault slip plane shown in Fig. 2C, it is limited at either end by two gullies and their associated dejection cones showing rocks, debris, and indicators of downslope transport on their surface (Figs. 2B, C). The video mosaic shows a distinct light-colored line that runs along the darker fault plane surface, mimicking the geometry of the present-day seafloor contact with this fault plane (Fig. 2D). While the fault

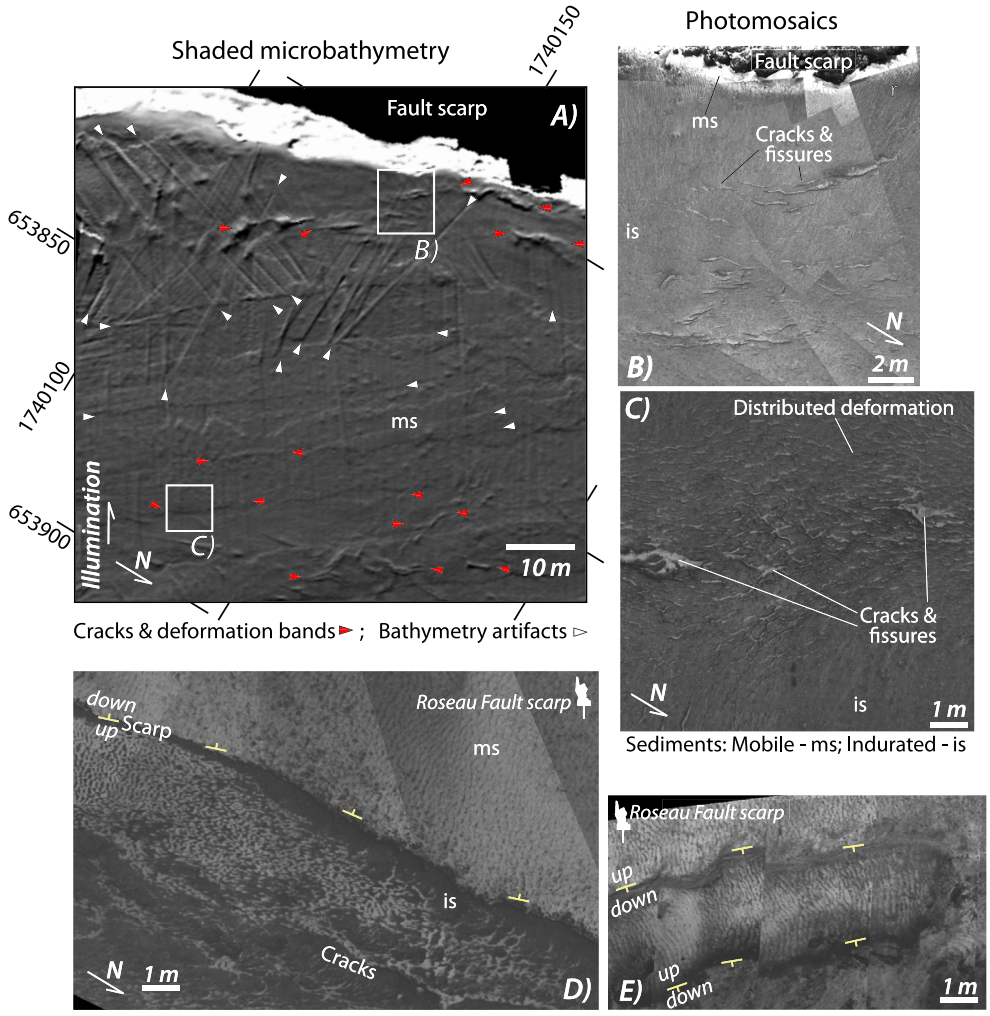



**Fig. 4.** Shaded microbathymetry (A) and seafloor photomosaics (B and C) from vertically acquired imagery showing cracks and fissures developing near the base of the fault scarp and deforming indurated sediments. The photomosaics also show small scarps (<1 m in vertical relief) dissecting the indurated sediment, and dipping both towards the Roseau fault (D) and away from it (E) which correspond to antithetic and synthetic faults in the hanging wall sediments. (For interpretation of the references to color in this figure, the reader is referred to the web version of this article.)

surface could not be sampled by the ROV, close-up high-definition video images suggest that this clear line is sediment adhered to the fault surface, which is coherent and indurated.

The video imagery also reveals a marked difference in the texture of the fault plane above and below this line (Figs. 3C, D). The surface below this line is dark, smooth, uncracked, and shows no sediment accumulation on surface irregularities. By contrast, above this line the surface is rough, displays numerous cracks, and has thin sediment dusting giving an overall lighter color to the fault surface (Figs. 3C–D). We attribute these textural distinctions to differential weathering, owing to shorter exposure to seawater of the lower part of the fault plane that is likely a recent fault exposure. We exclude erosion of hangingwall material exposing the previously buried fault scarp as a mechanism to produce such feature, as this process would obliterate the sediment line on the fault plane, which is also located between two gullies and preserved from erosion.

The smooth ribbon at the base of the fault scarp is likely produced by episodic slip on the fault rather than continuous aseismic slip. This is demonstrated by the difference in the weathering of the fault surface above and below the sediment line; the surface does not show a continuous weathering gradient. This fresh submarine surface exposure is similar to the freshly exposed coseismic scarps along subaerial faults following seismic events (Boncio et al., 2012; Cello et al., 2000; Smith et al., 2011). A coseismic origin, with a postseismic contribution discussed later, is indicated by the line of adhered sediment along most of this slip surface, by the geometry of this sediment line mimicking the present-day intersection of the fault plane with the seafloor, and by its weathering texture. Differential weathering of fault plane sections exposed through successive coseismic displacements has also been reported in normal subaerial faults (Giaccio et al., 2003; Wiatr et al., 2015).

We measure a maximum vertical displacement of ~0.9 m, corresponding to the height of the earthquake-related scarp (Fig. 2E), using the video-derived three-dimensional terrain model and the associated texture-mapped imagery (Campos et al., 2015). This apparent displacement tapers down to ~0.5 m laterally and towards the adjacent dejection cone. A 50% variation in fault slip over distances of a few meters is tectonically unrealistic. Instead, the dejection cone may have been reactivated during or following the observed fault slip, partially burying the scarp. Higher sedimentation rates near the mouth of the gully feeding this cone would result in an apparent decrease of displacement as observed in Fig. 3C. The absence of deformation structures along gully channels adjacent to the two fault slip planes shown in Fig. 2B indicates their efficient obliteration by the reactivation of erosion and sedimentation along the channel. The ~0.9 m vertical displacement is thus

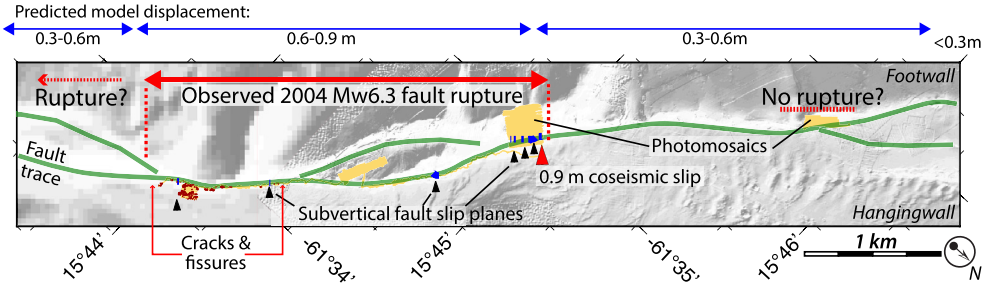



**Fig. 5.** Geometry of the Roseau normal fault trace within the survey area (green line), and associated distribution of coseismic deformation structures. Hangingwall cracks (dark red, see Fig. 4), together with the coseismic displacement along a slip surface (red triangle, see Fig. 3) indicates a minimum fault rupture of ~3 km (thick red line with arrowheads). The location of subvertical fault slip planes throughout the study area is also indicated (black small triangles). The rupture may extend to the southeast (dashed line with arrowhead), and terminate towards the northwest and within our study area (dashed red line). Models of fault displacements (thin blue lines with arrowheads above) based on earthquake sources (Feuillet et al., 2011a) underpredict the magnitude of observed coseismic slip, and the location of the maximum displacement is located southeast of the observed ~0.9 m of coseismic slip. (For interpretation of the references to color in this figure legend, the reader is referred to the web version of this article.)

a minimum estimate of the actual fault slip in this section of the fault, as the earthquake-related exposed fault plane may be partly buried by the reactivated dejection cone.

### 4.4. Hangingwall deformation structures

Seafloor photomosaics and oblique video imagery show numerous near-fault damage structures at the sedimented hangingwall along the base of the Roseau fault scarp. The hangingwall at the scarp base shows a dark, indurated, and ubiquitously rippled sediment layer. Locally, light colored, unconsolidated rippled sediments concentrate along the base of the fault scarp and in low-lying areas, such as the creases of ripples and bottoms of cracks (Fig. 4B). Along 1 km of the Roseau fault we observe that the indurated sediment is locally cracked and fissured (Fig. 4B), with zones of pervasive deformation hosting dense, coalescing crack networks extending over several tens of meters (Fig. 4C). The distribution of the cracks and fissures documenting near-fault hangingwall deformation along the fault trace are shown in Fig. 5.

Most of the photomosaic survey was conducted over the hangingwall in the immediate vicinity (within 10–20 m) of the fault scarp base (Fig. 1). We surveyed a zone ~150 m along the fault strike and ~110 m perpendicular to it that displays significant sediment cracking, fissuring, and deformation. These deformation structures here extend up to ~100 m away from the fault trace, suggesting that the hangingwall damage zone is broad, at least locally. The largest fractures are several meters long, several decimeters wide, and up to 30–50 cm deep, and are readily identifiable in the ROV microbathymetry (Fig. 4A). The smaller fractures, which can only be identified in the photomosaics, have lengths of a few cm, form dense clusters 1–5-m wide, and represent deformation belts that extend several tens of meters laterally (Fig. 4C).

Finally, north of the fissured hangingwall area we observe that the indurated sediment layer within the hangingwall is cut by scarps facing both towards the fault (Fig. 4D), and away from it (Fig. 4E). These scarps are found in sediments at distances of up to ~50 m from the base of the Roseau fault, and along the entire length of the fault that we surveyed with the photomosaics (Figs. 1 and 4). Their relief is relatively small, with a maximum of a few tens of centimeters, and in some cases they are found in association with cracking of the indurated sediment layer (Fig. 4D). We infer these scarps to be associated with both antithetic (Fig. 4D) and synthetic faults (Fig. 4E) induced by recent slip along the Roseau Fault, owing to their linearity, their proximity to the Roseau Fault trace, and their link to sediment cracks. While the photomosaic and visual coverage are limited (Fig. 2B), the observed cracks seem to be co-located with changes in the orientation of the Roseau Fault trace (Fig. 5), and thus may be associated with inhomogeneous deformation of the hangingwall above a complex fault plane geometry at depth. Fig. 6 shows the main features described here and their link to co-seismic and possibly post-seismic deformation.

## 5. Discussion and conclusions

### 5.1. The 2004 $M_w$ 6.3 Les Saintes earthquake and coseismic vs. postseismic deformation

The 2004 $M_w$ 6.3 Les Saintes earthquake is the only plausible cause for both the ~0.9 m vertical slip event recorded at the fault surface (Fig. 3), and the hangingwall deformation observed along the Roseau Fault trace (Fig. 4). First, the sediment line adhered to the fault surface (Fig. 3) that defines the earthquake-induced slip is an important chronological indicator, as it cannot be preserved over long periods of time (hundreds of years or more), owing to deep-sea currents, erosion, and submarine weathering. Second, these currents efficiently mobilize sediments from the Les Saintes Plateau towards the deepest sections of the Roseau Trough. This along-fault sediment transport is responsible for the accumulation of a thick sedimentary sequence (>300 m) at the center of the Roseau Fault (Leclerc et al., in press), as indicated by the rippled surface of both recent mobile and older indurated sediments (Fig. 4). While we have no accurate estimates of sedimentation rates in the area, a hemipelagic sedimentation rate of 0.5 mm/yr has been estimated in a similar basin along the Lesser Antilles volcanic arc (Beck et al., 2012), and is thus a minimum for our study area. Therefore, the cracks in the hangingwall as well as the secondary synthetic and antithetic structures are necessarily very recent, and are not long-lasting structures.

We conclude that the vertical offset measured along the fault is thus related to the 2004 earthquake. As our observations were made only nine years after the 2004 event, the offset may correspond primarily to a coseismic displacement, though potentially with an additional component of displacement due to post-seismic deformation (i.e. aftershocks and after-slip). Postseismic slip can represent up to 10–30% of the coseismic slip both along certain strike-slip and normal faults (Çakir et al., 2003; Cheloni et al., 2014). Assuming a similar range of 10–30% of post-seismic slip for Les Saintes, the post seismic slip may therefore have contributed ~−0.1–0.2 m of the observed 0.9, with a minimum coseismic slip of 0.7 m (Figs. 6A and B).

However, the postseismic slip induced by aftershocks could also be negligible along the Roseau Fault at the seafloor; the 2004 aftershock sequence was concentrated at a depth of about 10 km below our measurement site, and the main aftershocks did not produce any tsunami, therefore suggesting no surface break. Although afterslip can occur at the surface during the postseismic period (e.g.,

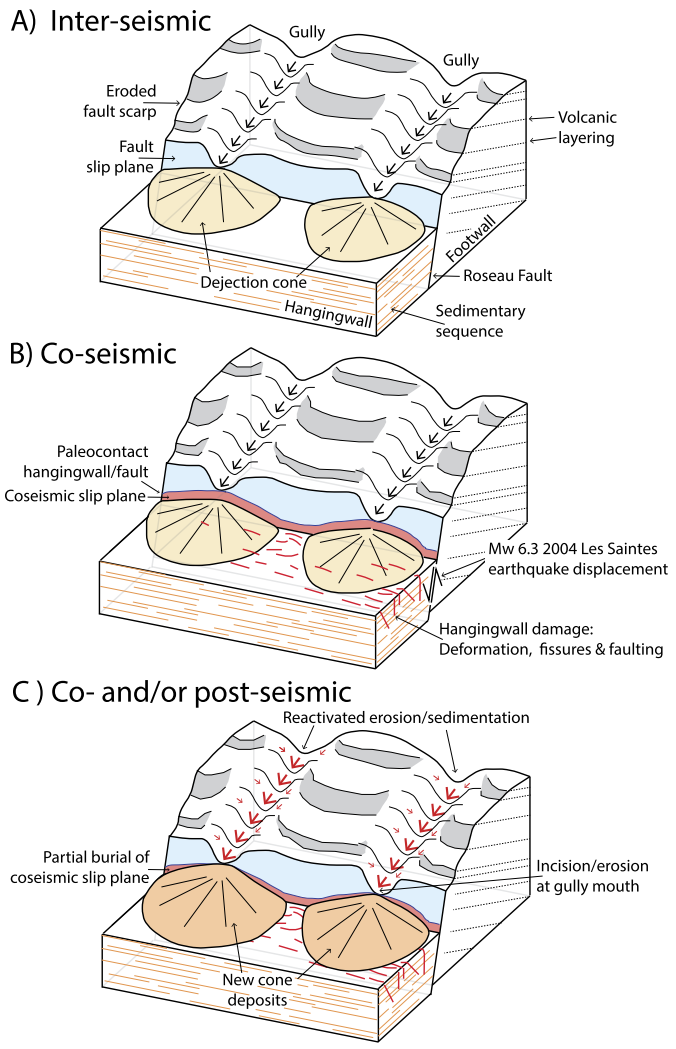



**Fig. 6.** Sketch of the features observed along the Roseau fault and their development associated with co-seismic and/or post seismic deformation. The fault slip plane is preserved between mouths of gullies, and newly exposed during seismic events. Coseismic deformation also induces fissuring and faulting of sediments in the hangingwall near fault. Erosion and sedimentation on dejection cones at the mouth of gullies is reactivated co- or post-seismically. The fault scarp is eroded over time, and the footwall internal volcanic layering is revealed by the stepped morphology of the scarp.

Smith and Wyss, 1968), other studies reveal that afterslip is mainly distributed at the edge of, and below the coseismic rupture, such as that documented following the L'Aquila 2009 $M_w$ 6.3 normal fault earthquake (Cheloni et al., 2014). If this post-seismic deformation pattern applies to the Roseau Fault, afterslip at the location of our observations (Fig. 3) could be either extremely limited or absent at the surface. That postseismic deformation here makes only a minor contribution is also supported by afterslip models based on friction laws (Marone et al., 1991), which show proportionally more afterslip occurring where surface coseismic slip is small relative to the deep coseismic slip. Our data cannot determine the presence or absence of postseismic slip and its amplitude here, but we conclude that it represents a proportion (probably less than ~10 cm) of the final vertical offset that we observed at the surface (~0.90 m) at this location (Fig. 3).

### 5.2. Constraints on the seismic history of the Roseau Fault

The vertical fault slip of at least 0.9 m that we have imaged (Fig. 3) provides constraints on the seismic history of the Roseau Fault scarp, and on the magnitude of the seismic event that caused it. While available empirical relationships between fault displacement and magnitude are based on subaerial observations (e.g., Bonilla et al., 1984; Wells and Coppersmith, 1994), as discussed further below, a displacement of almost ~1 m requires a large-magnitude event ($M_w$ > 5–6), such as the $M_w$ 6.3 2004 Les Saintes earthquake. The association of ephemeral indicators of coseismic displacement to the 2004 event is also supported by estimates of recurrence intervals for seismic events of similar magnitude and with similar slip. First, if a maximum long-term slip rate of 1 mm/yr for this fault is considered, as discussed elsewhere (Leclerc et al., in press), the recurrence interval for seismic events of similar magnitude and with similar slip is longer than a few hundreds of years. Second, there is no record of seismic events of similar magnitude both in instrumental or historical records (Feuillet et al., 2011a, 2011b), suggesting the recurrence interval must be a few hundreds of years or more.

We thus infer that the smooth ribbon at the base of the slip plane and bound by the adhered sediment line can only be related to the 2004 event, and that earlier events are not recorded owing to long-term exposure to seawater and associated weathering of the slip plane (Fig. 6B). These markers of coseismic displacement are comparable to weathering-induced patterns on active continental normal faults (Giaccio et al., 2003; Wiatr et al., 2015). While we have no constraint on the nature or rate of weathering observed on the slip plane, the lack of any apparent gradient in weathering above the most recent seismic event (Figs. 3D, E), which is observed in subaerial faults (Giaccio et al., 2003), suggests that weathering takes place at timescales shorter than the recurrence interval of seismic events. The subvertical fault slip planes preserved at Roseau scarp base (Figs. 2, 3 and 5) thus record cumulative fault displacement over several seismic cycles (i.e., over a few thousands of years). This is based on their height (up to ~10 m), the coseismic slip (~1 m) from large-magnitude ($M_w$ > 6) earthquakes, and the inferred recurrence time (0.5–1 kyr). These long recurrence intervals at the Roseau Fault are comparable to those inferred for some active, normal continental faults such as the 0.7–3.1 kyrs of the Magnola Fault (Carcaillet et al., 2008) or the ~0.2 kyrs of the Irpina Fault (Galli and Peronace, 2014).

### 5.3. Seafloor observation vs. model predictions of seafloor rupture parameters

Numerical models of fault rupture give first-order estimates of fault displacement and rupture length (Feuillet et al., 2011a; Le Friant et al., 2008). These estimates rely on numerous model assumptions, and lack any ground truthing. Using the near-fault wall damage zone structures, and the location of the fault plane showing coseismic slip, we document rupture along ~3 km of the Roseau Fault, as shown in Fig. 5. Our results provide ground-truth constraint that should be used to update and improve current models, as the model predictions show discrepancies with respect to the actual coseismic rupture geometry observed at the seafloor. The ~3 km of rupture identified thus corresponds to approximately one-third of the 10-km long rupture predicted by models (Feuillet et al., 2011a).

The northwestern termination of the modeled rupture lies within our study area, but we have identified no recent seafloor deformation structures in the visual and photomosaic surveys conducted (Fig. 1B and Fig. 5). This may suggest that the rupture did not actually propagate that far north at the surface, and that the model tsunami source (Le Friant et al., 2008) may therefore be inaccurate along this portion of the Roseau fault. At the southeastern limit of our survey area we find damage extending ~100 m from the fault scarp into the hangingwall. This suggests that the rupture

may have extended further to the southeast, and that the rupture is likely longer than the ~3 km observed although still shorter than the ~10 km proposed by the models.

The observed 0.9 m of coseismic displacement at a fault slip plane (Fig. 3) also shows discrepancies of the models with respect to field observations. The actual displacement may be greater than the observed 0.9 m, owing to the likely reactivation of the dejection cone during the 2004 earthquake discussed above, which may have partially buried the fault outcrop. While the maximum displacement predicted by models along the Roseau Fault (0.6–0.9 m) is comparable to the observed coseismic displacement (~0.9 m), these are not collocated: the fault section with predicted maximum displacement lies towards the southwest of the fault plane outcrop imaged here (Fig. 3). Instead, in the area of the observed fault slip planes, the predicted displacements are somewhat lower (0.3–0.6 m; Fig. 5). It is thus possible that the actual rupture is shorter than the ~10 km predicted by existing models. If this is the case, the overall displacement at the seafloor should be larger than that predicted by the same models for a seismic event of a given magnitude, which is consistent with the differences between observations and model predictions outlined above. While the data presented here provide some initial constraints on the 2004 Les Saintes earthquake coseismic rupture, they are of limited spatial extent. Additional observations are required to fully characterize the length and geometry of coseismic rupture, map the variations in width of the deformation zone in the hangingwall, and inspect additional fault slip planes, to obtain a complete distribution of coseismic fault displacement profile along the Roseau Fault. Nevertheless, the limited, available seafloor observations presented here demonstrate that models of rupture and tsunami source at Les Saintes require a reassessment, and that acquiring additional data along this and other fault systems is necessary to fully understand submarine fault ruptures and improve associated models.

### 5.4. Comparison with subaerial ruptures and scaling laws

The deformation structures observed at the seafloor along the Roseau Fault can be compared with structures associated with coseismic ruptures in subaerial faults. Such comparisons can help assess whether deformation and rupture processes are similar or differ fundamentally between these two environments, owing to differences in the environmental conditions and their effects on the rheology of both the fault and the surrounding materials. For example, the presence of water trapped in poorly connected cracks and pores during deformation events could result in elevated fluid pressures, weakening the fault zone, and promoting seismic rupture. Further, the elevated water pressure acting on the seafloor (~10 MPa) could promote a velocity weakening behavior in the shallowest portion of the fault, by helping the consolidation of otherwise loose near-surface material (Marone et al., 1991; Scholz, 1998). Such a mechanism would help propagate rupture pulses all the way to the seafloor instead of damping or halting them.

Normal subaerial faults with exhumed footwall bedrock often display ribbons of freshly exposed fault plane following seismic events (e.g., Cello et al., 2000; Pantosti et al., 1993; Vittori et al., 2011), as now also observed at the Roseau Fault slip plane (Fig. 3). These features are quickly obliterated on-land owing to rainfall, erosion, and other processes modifying the surface at rates much faster than in submarine environments. Near-fault coseismic deformation of the Roseau Fault hangingwall is also comparable to that observed subaerially. Normal faults in volcanic areas often feature shallow sub-vertical fault planes, with the formation of open fissures, fractures, and antithetic and synthetic faults along the hangingwall and next to scarps (e.g., Acocella et al., 2003; Martel and Langley, 2006). Inelastic near-fault deformation in subaerial faults also deforms the overlying sedimentary cover, as observed in association with normal, reverse, and strike-slip events (Baker et al., 2013; Boncio et al., 2012).

Subaerial observations further suggest changes in the width of the deformation zone along the fault trace, with increases in width correlating with complexities in the geometry of the fault (Boncio et al., 2012). We can estimate a minimum deformation width of ~100 m in the hangingwall of the Roseau Fault (Fig. 4), but cannot determine variations in deformation width along the fault scarp owing to our limited photomosaic coverage (Fig. 1B). This deformation width is consistent with those from observations at subaerial normal faults showing typical rupture widths over distances of <100 m and up to ~300 m from the fault, that also concentrate primarily along the hangingwall (Boncio et al., 2012). While our detailed submarine observations are restricted to a single coseismic rupture, they suggest that deformation processes such as hangingwall deformation and localization of deformation on slip fault planes (Figs. 6A and B) are, to a first order, similar to those observed onland. Finally, the apparent reactivation of erosion and sedimentation processes (Fig. 6C) suggests that seismicity may significantly contribute to the long-term erosion of the Roseau and nearby fault scarps, as observed onland (Keefer, 1994).

Fig. 7 shows relationships between seismic event magnitude and surface rupture length, as well as maximum displacement for a compilation of subaerial faults, to be compared with our observations at the Roseau Fault. These plots confirm that existing scaling laws (Wells and Coppersmith, 1994; Wesnousky, 2008) show sizable scatter, likely reflecting geological complexity of these systems. Because of this variability, rupture length and displacement can vary by a factor of 10 at a given seismic magnitude. In comparison, the single submarine observation of the Roseau Fault seems to have a relatively short rupture length, wether the modeled (Feuillet et al., 2011a; Le Friant et al., 2008) and the observed (this study) rupture lengths are considered (Fig. 7A). This rupture is associated with a large observed displacement (Fig. 7B), and hence a high displacement-length ratio compared to subaerial faults. While we can speculate that this high displacement-length ratio may be linked to near-surface displacement facilitated by hydrostatic pressure and the presence of fluids, additional data from other submarine faults is required to evaluate the robustness of differences between submarine and subaerial fault ruptures.

## 6. Conclusions

Understanding the dynamics of coseismic fault rupture and the associated inelastic processes requires detailed studies along submarine faults. These data thus provide a first submarine observation that can be integrated with existing compilations linking surface rupture geometry to earthquake magnitude, that are now based exclusively on subaerial fault rupture. More than two thirds of the Earth's seismicity takes place in the oceans, with a sizable proportion in proximity to coastal areas, where there is a combined seismic and tsunami hazard.

With this study we demonstrate that underwater vehicles can conduct geophysical surveys and geological observations at spatial scales similar to that of subaerial studies, and that systematic and routine seafloor observations in subaqueous environments can be conducted using advanced acoustic (Fig. 2) and optical (Figs. 3 and 4) imaging techniques. Along the Roseau fault these methods reveal recent deformation structures that we can link to the submarine 2004 $M_w$ 6.3 Les Saintes earthquake. We document a surface rupture length of at least ~3 km that does not prolong as far north as previously modeled, and whose length is likely shorter than the ~10–15 km rupture length proposed by earlier models. We also identify coseismic displacement at a preserved fault slip

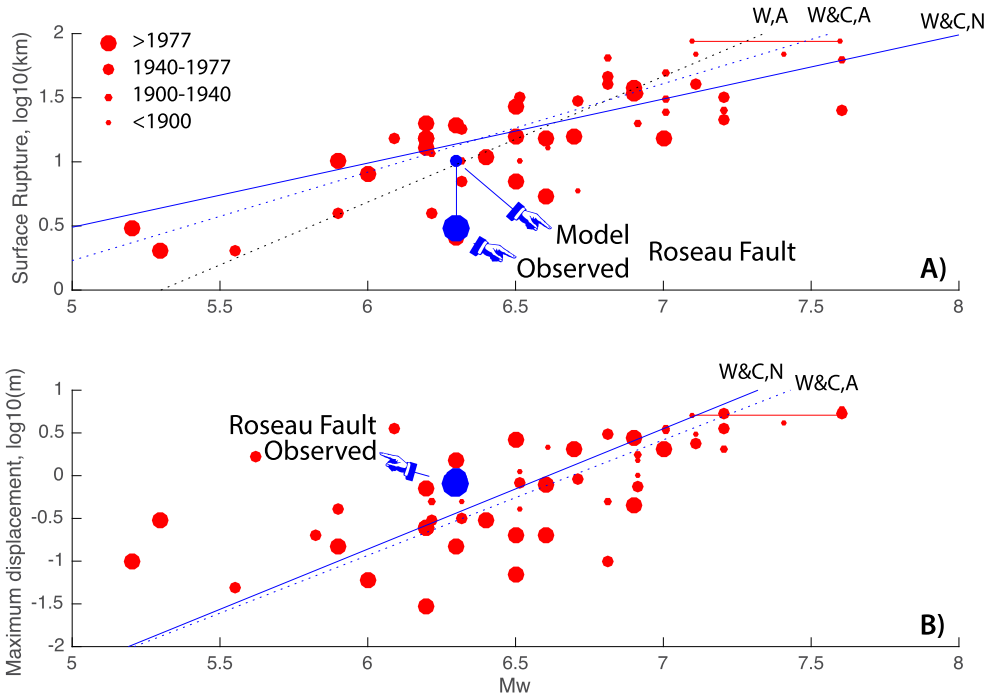



**Fig. 7.** Earthquake magnitude vs. surface rupture length (A) and maximum displacement (B) of subaerial normal faults (red circles) compared with the submarine observations along the Roseau Fault rupture (large blue dots) and model estimates (small blue dot). Subaerial observations range from instrumental records (1977 and later, largest circles) to pre-instrumental historical events (1900 and earlier, smallest circles). Selected magnitude scaling laws, labeled W&C (Wells and Coppersmith, 1994) and W (Wesnousky, 2008) are also plotted for normal faults (N, solid lines) and for all faults combined (A, dotted lines). The data used in this plot, together with corresponding references, are provided in Supplementary Table 1. (For interpretation of the references to color in this figure legend, the reader is referred to the web version of this article.)

surface, with a maximum displacement of 0.9 m. This is somewhat higher than that predicted by models, and not collocated with the predicted zone of maximum displacement. Our observations also indicate that erosion of the fault plane along gullies, and concomitant sedimentation on dejection cones at their mouths, is efficient and may occur co-seismically, post-seismically, or both.

The coseismic deformation structures observed at the seafloor, both on fault slip planes and on the hangingwall, are similar to those observed along subaerial ruptures. We are able to identify well preserved seafloor ruptures ~10 yrs after their formation (Figs. 2–5) owing to submarine erosion and weathering rates that are in general less efficient than those operating on land. Hence, the techniques used here open the possibility of conducting additional, extensive high-resolution underwater surveys along fault scarps that have witnessed earthquake ruptures in recent times, but that have not been characterized to date. Such offshore studies would allow us to better document and enrich existing seismic catalogs that are used for semi-empirical scaling laws (Wells and Coppersmith, 1994; Wesnousky, 2006; 2008), which lack underwater seismic events and under-represent normal and thrust seismic ruptures. By doing so we could improve the assessment of seismic and tsunami hazards associated with earthquakes in oceanic areas.

## Author contributions

Data were acquired by the cruise participants (NA, AB, DB, VC, YC, MG, KH, CH, BI, JJ, BJ, FL, TL, CJM, MM-C, PN, JAO, SP, AS, MT, LT), led by JE. The experiment was planned and designed by JE, MC, FL, CD, NF, and MA. Processing of microbathymetry data was conducted by NA, MR, AS and GV, in coordination with SV, JE, and MC. Imagery was processed by RP, RG, NG, and JE. Data interpretation was coordinated by JE, and involved all participants. The manuscript was drafted by JE, FL, CM, and JAO, with input from the rest of co-authors.

## Acknowledgements

Data presented in this paper were acquired during the ODEMAR Cruise with trip time and ROV deployment funded by CNRS and IFREMER (France), with AUV deployments funded by GEOMAR (Germany). CNRS provided support for data analyses through an INSU-SYSTER grant to JE. CJM's participation was funded by NERC grant NE/J021741/1 at Cardiff University. We thank X. Castrec (IFREMER) for facilitating permits and authorizations required for the fieldwork, and the GENAVIR Team and ship's crew and officers for all shipboard and ROV operations. Reviews provided by A. Robinson and an anonymous reviewer, in addition to those from the Editor An Yin, helped improve this manuscript. This is IPGP contribution 3757.

## Appendix A. Supplementary material

Supplementary material related to this article can be found online at http://dx.doi.org/10.1016/j.epsl.2016.06.024.

## References

Acocella, V., Korme, T., Salvini, F., 2003. Formation of normal faults along the axial zone of the Ethiopian Rift. J. Struct. Geol. 25, 503–513.

Armijo, R., Pondard, N., Meyer, B., Uçarkus, G., de Lépinay, B.M., Malavieille, J., Dominguez, S., Gustcher, M.-A., Schmidt, S., Beck, C., Çagatay, N., Çakir, Z., Imren, C., Eris, K., Natalin, B., Özalaybey, S., Tolun, L., Lefèvre, I., Seeber, L., Gasperini, L., Rangin, C., Emre, O., Sarikavak, K., 2005. Submarine fault scarps in the Sea of Marmara pull-apart (North Anatolian Fault): implications for seismic hazard in Istanbul. Geochem. Geophys. Geosyst. 6, Q06009.

Avouac, J.-P., Ayoub, F., Wei, S., Ampuero, J.-P., Meng, L., Leprince, S., Jolivet, R., Duputel, Z., Helmberger, D., 2014. The 2013, Mw 7.7 Balochistan earthquake, energetic strike-slip reactivation of a thrust fault. Earth Planet. Sci. Lett. 391, 128–134.

Baker, A., Allmendinger, R.W., Owen, L.A., Rech, J.A., 2013. Permanent deformation caused by subduction earthquakes in northern Chile. Nat. Geosci. 6, 492–496.

Barreyre, T., Escartín, J., Garcia, R., Cannat, M., Mittelstaedt, E., Prados, R., 2012. Structure, temporal evolution, and heat flux estimates from the Lucky Strike deep-sea hydrothermal field derived from seafloor image mosaics. Geochem. Geophys. Geosyst. 13, Q04007.

Bazin, S., Feuillet, N., Duclos, C., Crawford, W., Nercessian, A., Bengoubou-Valérius, M., Beauducel, F., Singh, S.C., 2010. The 2004–2005 Les Saintes (French West Indies) seismic aftershock sequence observed with ocean bottom seismometers. Tectonophysics 489, 91–103.

Beck, C., Reyss, J.L., Leclerc, F., Moreno, E., Feuillet, N., Barrier, L., Beauducel, F., Boudon, G., Clément, V., Deplus, C., Gallou, N., Lebrun, J.F., Le Friant, A., Nercessian, A., Paterne, M., Pichot, T., Vidal, C., 2012. Identification of deep subaqueous co-seismic scarps through specific coeval sedimentation in Lesser Antilles: implication for seismic hazard. Nat. Hazards Earth Syst. Sci. 12, 1755–1767.

Bhat, H.S., Dmowska, R., King, G.C.P., Klinger, Y., Rice, J.R., 2007. Off-fault damage patterns due to supershear ruptures with application to the 2001 Mw 8.1 Kokoxili (Kunlun) Tibet earthquake. J. Geophys. Res., Solid Earth 112, B06301.

Boncio, P., Galli, P., Naso, G., Pizzi, A., 2012. Zoning surface rupture hazard along normal faults: insight from the 2009 Mw 6.3 L'Aquila, Central Italy, earthquake and other global earthquakes. Bull. Seismol. Soc. Am. 102, 918–935.

Bonilla, M.G., Mark, R.K., Lienkaemper, J.J., 1984. Statistical relations among earthquake magnitude, surface rupture length, and surface fault displacement. Bull. Seismol. Soc. Am. 74, 2379–2411.

Çakir, Z., Chabalier, J.-B., de Armijo, R., Meyer, B., Barka, A., Peltzer, G., 2003. Coseismic and early post-seismic slip associated with the 1999 Izmit earthquake (Turkey), from SAR interferometry and tectonic field observations. Geophys. J. Int. 155, 93–110.

Campos, R., Garcia, R., Alliez, P., Yvinec, M., 2015. A surface reconstruction method for in-detail underwater 3D optical mapping. Int. J. Robot. Res. 31, 64–89.

Cara, M., Bertil, D., Feuillet, N., Jacques, E., Tapponnier, P., Guéguen, P., Bengoubou-Valérius, M., Sira, C., Lebrun, B., Beauducel, F., 2005. Séisme des Saintes (Guadeloupe) du 21 novembre 2004. Strasbourg, France.

Carcaillet, J., Manighetti, I., Chauvel, C., Schlagenhauf, A., Nicole, J., 2008. Identifying past earthquakes on an active normal fault (Magnola, Italy) from the chemical analysis of its exhumed carbonate fault plane. Earth Planet. Sci. Lett. 271, 145–158.

Cattaneo, A., Babonneau, N., Ratzov, G., Dan-Unterseh, G., Yelles, K., Bracène, R., Mercier de Lépinay, B., Boudiaf, A., Déverchère, J., 2012. Searching for the seafloor signature of the 21 May 2003 Boumerdès earthquake offshore central Algeria. Nat. Hazards Earth Syst. Sci. 12, 2159–2172.

Cello, G., Deiana, G., Ferelli, L., Marchegiani, L., Maschio, L., Mazzoli, S., Michetti, A., Serva, L., Tondi, E., Vittori, T., 2000. Geological constraints for earthquake faulting studies in the Colfiorito area (central Italy). J. Seismol. 4, 357–364.

Cheloni, D., Giuliani, R., D'Anastasio, E., Atzori, S., Walters, R.J., Bonci, L., D'Agostino, N., Mattone, M., Calcaterra, S., Gambino, P., Deninno, F., Maseroli, R., Stefanelli, G., 2014. Coseismic and post-seismic slip of the 2009 L'Aquila (central Italy) Mw 6.3 earthquake and implications for seismic potential along the Campotosto fault from joint inversion of high-precision levelling, InSAR and GPS data. Tectonophysics 622, 168–185.

DePolo, C., Clark, D., Slemmons, D.B., Ramelli, R., 1991. Historical surface faulting in the Basin and Range province, western North America: implications for fault segmentation. J. Struct. Geol. 13, 123–136.

Elias, A., Tapponnier, P., Singh, S.C., King, G.C.P., Briais, A., Daëron, M., Carton, H., Sursock, A., Jacques, E., Jomaa, R., Klinger, Y., 2007. Active thrusting offshore Mount Lebanon: source of the tsunamigenic A.D. 551 Beirut–Tripoli earthquake. Geology 35, 755.

Fabbri, O., Fournier, M., 1999. Extension in the southern Ryukyu arc (Japan): link with oblique subduction and back arc rifting. Tectonics 18, 486–497.

Feuillet, N., Beauducel, F., Jacques, E., Tapponnier, P., Delouis, B., Bazin, S., Vallée, M., King, G.C.P., 2011a. The Mw = 6.3, November 21, 2004, Les Saintes earthquake (Guadeloupe): tectonic setting, slip model and static stress changes. J. Geophys. Res. 116, B10301.

Feuillet, N., Beauducel, F., Tapponnier, P., 2011b. Tectonic context of moderate to large historical earthquakes in the Lesser Antilles and mechanical coupling with volcanoes. J. Geophys. Res. 116, B10308. http://dx.doi.org/10.1029/2011JB008443.

Feuillet, N., Leclerc, F., Tapponnier, P., Beauducel, F., Boudon, G., Le Friant, A., Deplus, C., Lebrun, J.-F., Nercessian, A., Saurel, J.-M., Clément, V., 2010. Active faulting induced by slip partitioning in Montserrat and link with volcanic activity: new insights from the 2009 GWADASEIS marine cruise data. Geophys. Res. Lett. 37, L00E15. http://dx.doi.org/10.1029/2010GL042556.

Feuillet, N., Manighetti, I., Tapponier, P., Jaqcques, E., 2002. Arc parallel extension and localization of volcanic complexes in Guadeloupe, Lesser Antilles. J. Geophys. Res. 107 (B12), 2156–2202. http://dx.doi.org/10.1029/2001JB000308.

Fujiwara, T., Kodaira, S., No, T., Kaiho, Y., Takahashi, N., Kaneda, Y., 2011. The 2011 Tohoku-Oki earthquake: displacement reaching the trench axis. Science 334, 1240.

Galgana, G., Hamburger, M., McCaffrey, R., Corpuz, E., Chen, Q., 2007. Analysis of crustal deformation in Luzon, Philippines using geodetic observations and earthquake focal mechanisms. Tectonophysics 432, 63–87.

Galli, P., Peronace, E., 2014. New paleoseismic data from the Irpinia Fault. A different seismogenic perspective for southern Apennines (Italy). Earth-Sci. Rev. 136, 175–201. http://dx.doi.org/10.1016/j.earscirev.2014.05.013.

Giaccio, B., Galadini, F., Sposato, A., Messina, P., Moro, M., Zreda, M., Cittadini, A., Salvi, S., Todero, A., 2003. Image processing and roughness analysis of exposed bedrock fault planes as a tool for paleoseismological analysis: results from the Campo Felice fault (central Apennines, Italy). Geomorphology 49, 281–301.

Goldfinger, C., 2011. Submarine paleoseismology based on turbidite records. Ann. Rev. Mar. Sci. 3, 35–66.

Keefer, D.K., 1994. The importance of earthquake-induced landslides to long-term slope erosion and slope-failure hazards in seismically active regions. Geomorphology 10, 265–284.

King, G., 2005. Slip-partitioned surface breaks for the Mw 7.8 2001 Kokoxili earthquake, China. Bull. Seismol. Soc. Am. 95, 731–738.

Klinger, Y., 2005. High-resolution satellite imagery mapping of the surface rupture and slip distribution of the Mw 7.8, 14 November 2001 Kokoxili Earthquake, Kunlun Fault, Northern Tibet, China. Bull. Seismol. Soc. Am. 95, 1970–1987.

Kodaira, S., No, T., Nakamura, Y., Fujiwara, T., Kaiho, Y., Miura, S., Takahashi, N., Kaneda, Y., Taira, A., 2012. Coseismic fault rupture at the trench axis during the 2011 Tohoku-Oki earthquake. Nat. Geosci. 5, 646–650.

Le Friant, A., Heinrich, P., Boudon, G., 2008. Field survey and numerical simulation of the 21 November 2004 tsunami at Les Saintes (Lesser Antilles). Geophys. Res. Lett. 35, L12308. http://dx.doi.org/10.1029/2008GL034051.

Leclerc, F., 2014. Déformation active permanente induite par le méga-chevauchement dans l'arc antillais: apport des complexes récifaux quaternaires. Institut de Physique du Globe de Paris, Sorbonne Paris Cité.

Leclerc, F., Feuillet, N., Cabioch, G., Deplus, C., Lebrun, J.F., Bazin, S., Beauducel, F., Boudon, G., LeFriant, A., De Min, L., Melezan, D., 2014. The Holocene drowned reef of Les Saintes plateau as witness of a long-term tectonic subsidence along the Lesser Antilles volcanic arc in Guadeloupe. Mar. Geol. 355, 115–135.

Leclerc, F., Feuillet, N., Deplus, C., in press. Interactions between active faulting, volcanism, and sedimentary processes at an island arc: insights from Les Saintes channel, Lesser Antilles arc. Geochem. Geophys. Geosyst. http://dx.doi.org/10.1002/2016GC006337. http://onlinelibrary.wiley.com/doi/10.1002/2016GC006337/full.

Marano, K.D., Wald, D.J., Allen, T.I., 2010. Global earthquake casualties due to secondary effects: a quantitative analysis for improving rapid loss analyses. Nat. Hazards 52, 319–328.

Marone, C., Scholtz, C.H., Bilham, R., 1991. On the mechanics of earthquake afterslip. J. Geophys. Res. 96, 8441–8452.

Martel, S.J., Langley, J.S., 2006. Propagation of normal faults to the surface in basalt, Koae fault system, Hawaii. J. Struct. Geol. 28, 2123–2143.

Matsumoto, T., Shinjo, R., Nakamura, M., 2009. Did the submarine, across-arc normal fault system in the Southwest Ryukyu Arc Trigger the 1771 tsunami? Field Evidence from Multibeam Survey and In-Situ. Pol. J. Environ. Stud. 18, 123–129.

Nicosevici, T., Garcia, R., 2013. Efficient 3D Scene Modeling and Mosaicing. Springer Verlag, ISBN 978-3-642-36417-4.

Pantosti, D., Schwartz, D.P., Valensise, G., 1993. Paleoseismology along the 1980 surface rupture of the Irpinia Fault: implications for earthquake recurrence in the southern Apennines, Italy. J. Geophys. Res. 98, 6561.

Papazachos, B.C., Scordilis, E.M., Panagiotopoulos, D.G., Papazachos, C.B., Karakaisis, G.F., 2004. Global relations between seismic fault parameters and moment magnitude of earthquakes. Bull. Geol. Soc. Greece XXXVI, 1482–1489.

Prados, R., Garcia, R., Gracias, N., Escartín, J., Neumann, L., 2012. A novel blending technique for underwater gigamosaicing. IEEE J. Ocean. Eng. 37. http://dx.doi.org/10.1109/JOE.2012.2204152.

Rockwell, T.K., Klinger, Y., 2013. Surface rupture and slip distribution of the 1940 Imperial Valley earthquake, Imperial Fault, Southern California: implications for rupture segmentation and dynamics. Bull. Seismol. Soc. Am. 103, 629–640.

Scholz, C.H., 1998. Earthquakes and friction laws. Nature 391, 37–42.

Scholz, C.H., Aviles, C.A., Wesnousky, S.G., 1986. Scaling differences between large interplate and intraplate earthquakes. Bull. Geol. Soc. Am. 76, 65–70.

Smith, S.A.F., Billi, A., Di Toro, G., Spiess, R., 2011. Principal slip zones in limestone: microstructural characterization and implications for the seismic cycle (Tre Monti Fault, Central Apennines, Italy). Pure Appl. Geophys. 168, 2365–2393.

Smith, S.W., Wyss, M., 1968. Displacement on the San Andreas fault subsequent to the 1966 Parkfield Earthquake. Bull. Seismol. Soc. Am. 58, 1955–1973.

Stock, C., Smith, E.G.C., 2000. Evidence for different scaling of earthquake source parameters for large earthquakes depending on faulting mechanism. Geophys. J. Int. 143, 157–162.

Tsuji, T., Ito, Y., Kawamura, K., Kanamatsu, T., Kasaya, T., Kinoshita, M., Matsuoka, T., YK11-04E Shipboard Scientists, YK11-06E Shipboard Scientists, 2012. Seismogenic faults of the 2001 Great East Japan Earthquake: insights from seismic data and seafloor observations. Proc. Int. Symp. Eng. Lessons Learn. from 2011 Gt. East Japan Earthq. 281–288.

Vittori, E., Di Manna, P., Blumetti, A.M., Comerci, V., Guerrieri, L., Esposito, E., Michetti, A.M., Porfido, S., Piccardi, L., Roberts, G.P., Berlusconi, A., Livio, F., Sileo, G., Wilkinson, M., McCaffrey, K.J.W., Phillips, R.J., Cowie, P.A., 2011. Surface faulting of the 6 April 2009 Mw 6.3 L'Aquila Earthquake in Central Italy. Bull. Seismol. Soc. Am. 101, 1507–1530.

Wells, D.L., Coppersmith, K.J., 1994. New empirical relationships among magnitude, rupture length, rupture width, rupture area and surface displacement. Bull. Seismol. Soc. Am. 84, 974–1002.

Wesnousky, S.G., 2006. Predicting the endpoints of earthquake ruptures. Nature 444, 358–360. http://dx.doi.org/10.1038/nature05275.

Wesnousky, S.G., 2008. Displacement and geometrical characteristics of earthquake surface ruptures: issues and implications for seismic-hazard analysis and the process of earthquake rupture. Bull. Seismol. Soc. Am. 98, 1609–1632.

Wiatr, T., Papanikolaou, I., Fernández-Steeger, T., Reicherter, K., 2015. Bedrock fault scarp history: insight from t-LiDAR backscatter behaviour and analysis of structure changes. Geomorphology 237, 119–129.